catalysts

MDPI

Article

Cross-Aldol Condensation of Acetone and *n*-Butanol into Aliphatic Ketones over Supported Cu Catalysts on Ceria-Zirconia

Minseok Kim [1], Jongha Park [1], Hari Prasad Reddy Kannapu [1,2] and Young-Woong Suh [1,2,*]

[1] Department of Chemical Engineering, Hanyang University, Seoul 04763, Korea; im.mkim87@gmail.com (M.K.); pakjongha@empas.com (J.P.); kannapuhari@gmail.com (H.P.R.K.)
[2] Research Institute of Industrial Science, Hanyang University, Seoul 04763, Korea
* Correspondence: ywsuh@hanyang.ac.kr; Tel.: +82-2-2220-2329

Academic Editor: Christophe Len
Received: 7 August 2017; Accepted: 23 August 2017; Published: 24 August 2017

Abstract: A long-chain hydrocarbon biofuel of jet fuel range can be produced via aldol condensation of fermented products such as acetone and alcohols over the catalysts containing both metallic sites for the dehydrogenation of alcohols and basic sites for the condensation reaction. However, an efficient catalyst system has not been studied widely yet the route is promising for biofuel production. In this work, Cu catalysts supported on ceria-zirconia (Cu/*x*CeZr) were prepared using coprecipitated $Ce_xZr_{1-x}O_2$ supports with different Ce/Zr ratios for the cross-aldol condensation of acetone and *n*-butanol into mono- and di-alkylated aliphatic ketones, 2-heptanone and 6-undecanone. The acetone conversion and 6-undecanone selectivity increased with specific Cu surface area due to formation of the dehydrogenation product butyraldehyde at a higher concentration. The total yield of cross-aldol condensation products was strongly dependent on a combination of Cu sites and basic sites. This was confirmed by the results in the reaction between acetone and butyraldehyde over supported Cu catalysts that additionally examined the adsorbed acyl species on Cu surface taking part in the aldol condensation reaction. The best catalytic performance was achieved with Cu/0.8CeZr showing the largest Cu surface and the highest base site density among Cu/*x*CeZr catalysts. While the activity of Cu/0.8CeZ was comparable to or a little higher than that of Cu/MgO, the former catalyst was more stable than the latter suffering from the transformation of MgO to $Mg(OH)_2$ by the reaction. Consequently, it is suggested that Cu supported on ceria-zirconia of ceria rich contains such a dual function that it can efficiently catalyze the cross-aldol condensation of acetone and *n*-butanol.

Keywords: copper; ceria-zirconia; dehydrogenation; cross-aldol condensation; basic sites

1. Introduction

Due to CO_2 emission and diminishing reserves of fossil fuels, carbon-neutral fuel alternatives have been attracting much attention in recent decades. A typical example is biofuel produced either by direct conversion such as fermentation, gasification, pyrolysis and liquefaction [1] or by indirect conversion based upon syncretic chemistry (i.e., combination of biological and chemical transformations) [2,3]. A promising route for the latter-related process has been recently proposed such that acetone, ethanol and butanol produced via anaerobic fermentation can be transformed into long-chain hydrocarbons of jet fuel range [4–8]. There are two important steps in this conversion; the first step is alcohol dehydrogenation into aldehyde over metallic sites and the second is aldol condensation between acetone of enol/enolate type (adsorbed acetone over basic sites) and in-situ formed aldehyde, finally resulting in mono- and di-alkylated aliphatic ketones. In case of the condensation reaction between

acetone and *n*-butanol, the desired products are 2-heptanone (C7) and 6-undecanone (C11), which are formed when a molar stoichiometry of acetone/*n*-butanol is 1:1 and 1:2, respectively.

This reaction requires two catalytic functions for the dehydrogenation of alcohol into aldehyde and for the condensation of acetone with aldehyde. The detailed reaction pathway is depicted in Scheme 1 including possible side reactions relevant to the conversion of *n*-butanol explained later. In the first report of Toste and coworkers [5], a noble metal-supported catalyst and basic K_3PO_4 were used together. Further study revealed a high performance of MgO–Al_2O_3 hydrotalcite as a basic support onto which Pd, Ru, and Cu (the most active) were loaded [6]. Moreover, they demonstrated how Cu/hydrotalcite and Pd-Cu/hydrotalcite catalysts affect the aldol condensation reaction and which elementary step is rate determining [7,8]. A series of their reports are very elegant and deliver helpful insight into catalytically active sites for the cross-aldol condensation of acetone and alcohols. However, their catalyst development has been limited to hydrotalcite as a support material.

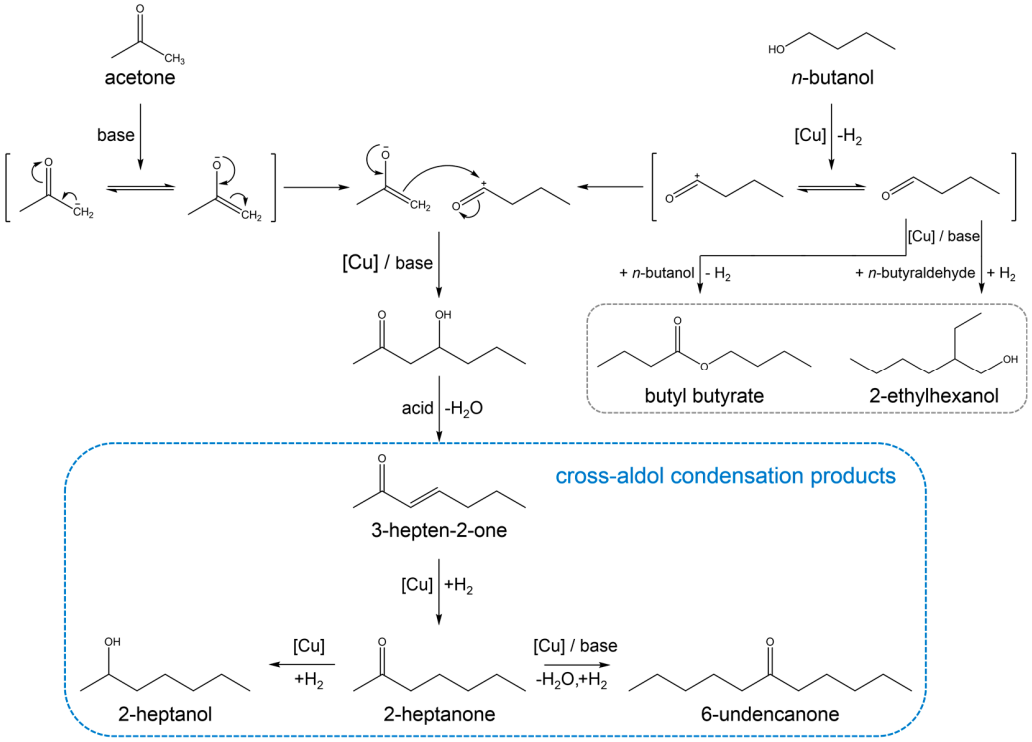

Scheme 1. Cross-aldol condensation of acetone and *n*-butanol.

In this work, we focus on ceria-zirconia mixed oxide ($Ce_xZr_{1-x}O_2$), since it proved to be effective in oxygenate coupling reactions such as ketonization and aldol condensation. Mallinson et al. reported that zirconia-rich $Ce_xZr_{1-x}O_2$ catalysts ($x < 0.5$) favored aldol condensation and ceria-rich ones ($x > 0.5$) formed more ketonization products in the condensation of propanal [9]. The reaction preference occurred by shifting a balance in the quantity and strength of $Ce_xZr_{1-x}O_2$'s Lewis acid-base sites pairs [10]. The Ce/Zr ratio of 1:1 was found to be optimum in catalyzing both ketonization and aldol condensation reactions, resulting from the best combination of each reaction activity as well as catalyst stability. This composition of ceria-zirconia catalyst has been used in upgrading light fractions of a simulated bio-oil [11], aldehyde [12], and carboxylic acids [13,14]. A catalyst consisting of Pd metal and $Ce_{0.5}Zr_{0.5}O_2$ support was also demonstrated to be stable and effective in the ketonization reaction [15–17]. However, these studies focused on the self-condensation reaction (i.e., condensation between the identical reactant molecules), which is unlike the reaction in this work involving a couple of alcohol dehydrogenation and cross-aldol condensation between acetone and in-situ formed aldehyde. On the other hand, the aldol condensation of acetone with furfural has been extensively investigated in recent years but $Ce_xZr_{1-x}O_2$ has never been used as a support [18].

Thus, $Ce_xZr_{1-x}O_2$ is used herein as a support for the cross-aldol condensation of acetone and *n*-butanol, and the activities of Cu catalysts supported on $Ce_xZr_{1-x}O_2$ are examined, which is the first report as far as we know. Note that Cu metal is selected for alcohol dehydrogenation because its high activity is already examined [19]. In the preparation of $Ce_xZr_{1-x}O_2$, supports hereafter referred to as *x*CeZr, the *x* value representing the [Ce]/{[Ce]+[Zr]} varies from 0 (pure ZrO_2) to 1 (pure CeO_2). For comparison, basic MgO and acidic Al_2O_3 are used as a support for Cu loading. Physical and chemical characteristics of all supports, calcined CuO samples, and reduced Cu catalysts are characterized by X-ray diffraction (XRD), Brunauer-Emmett-Teller (BET) method, H_2 temperature-programmed reduction (H_2-TPR), N_2O reactive frontal chromatography (N_2O-RFC), and temperature-programmed desorption of NH_3 and CO_2 (NH_3-TPD and CO_2-TPD). The acetone conversion and product selectivities are correlated with specific Cu surface area, acid/base site densities or a combination thereof. From this approach and the reaction results in the condensation of acetone and butyraldehyde, we intend to figure out key catalyst properties for the cross-aldol condensation of acetone and *n*-butanol. Finally, when compared with Cu/MgO in terms of the activity and stability, Cu supported on ceria-zirconia of ceria rich is considered to be catalytically active and stable in the reaction.

2. Results

2.1. Catalyst Characterization Results

For a series of *x*CeZr, calcined CuO/*x*CeZr, and reduced Cu/*x*CeZr samples with different *x* values, powder XRD patterns are presented in Figure 1. The patterns of pure supports 1CeZr and 0CeZr resemble the reflections of cubic ceria (JCPDS PDF#34-0394) and tetragonal zirconia (JCPDS PDF#27-0997), respectively. As the *x* value decreases to 0.2, the reflections of *x*CeZr samples are shifted to high angles, indicating the transition from the cubic fluorite to the tetragonal structure [20], and they are broadened due to small crystallite sizes. The latter finding is confirmed by the specific BET surface area (S_{BET}) summarized in Table 1. On the other hand, the symmetrical shape of all reflections for *x*CeZr with $x = 0.2$, 0.5, and 0.8 is due to no peak splitting by the presence of two phases, which suggests the formation of single ceria-zirconia solid solution [21]. These observations are similarly found in calcined CuO/*x*CeZr and reduced Cu/*x*CeZr samples, explaining that Cu loading and subsequent calcination/reduction rarely change the structure of ceria-zirconia support.

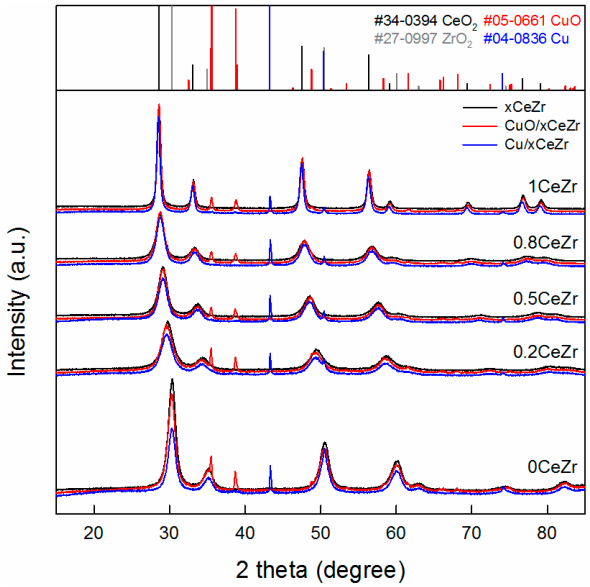

Figure 1. Powder X-ray diffraction patterns of *x*CeZr (black), calcined CuO/*x*CeZr (red), and reduced Cu/*x*CeZr (blue) samples. The reflections of CeO_2 (black bars), ZrO_2 (gray bars), CuO (red bars), and Cu metal (blue bars) are included for peak identification.

Table 1. Physical and chemical properties of *x*CeZr, CuO/*x*CeZr, and Cu/*x*CeZr samples.

	*x*CeZr	CuO/*x*CeZr		Cu/*x*CeZr				
	S_{BET} (m^2 g^{-1})	S_{BET} (m^2 g^{-1})	D_{CuO} [1] (nm)	S_{Cu} [2] (m^2 g_{Cu}^{-1})	D_{Cu} [2] (nm)	d_{Cu} [2] (%)	N_{CO2} [3] (μmol g^{-1})	N_{NH3} [3] (μmol g^{-1})
1CeZr	43	62	53	15.1	45	7.4	321.7	473.4
0.8CeZr	104	84	35	24.3	35	11.9	619.0	823.7
0.5CeZr	104	82	51	10.7	63	5.2	497.6	842.3
0.2CeZr	98	66	72	9.0	75	4.4	618.7	1183.2
0CeZr	102	57	78	5.2	131	2.5	560.4	944.2

[1] Calculated using the CuO(111) reflection at $2\theta = 38.8°$; [2] Calculated using the results of N_2O-RFC experiments; [3] Measured by TPD experiments using CO_2 and NH_3 for N_{CO2} and N_{NH3}, respectively.

In all XRD patterns of CuO/*x*CeZr, the reflections of CuO corresponding to tenorite (JCPDS PDF#05-0661) are detected at $2\theta = 35.5°$ and 38.8°. When calculated using the latter CuO(111) reflection by the Scherrer equation, the average particle size of CuO (D_{CuO}) is the smallest for CuO/0.8CeZr and the largest for CuO/0CeZr (Table 1). Thus, H_2-TPR measurement was conducted in order to study a reduction characteristic of CuO particles and also an interaction between metal oxide and support. In Figure 2, CuO/0CeZr exhibits a broad reduction peak with a maximum at 485 K, while CuO/1CeZr shows the similar peak at 494 K together with a small hump at 417 K. The broad reduction peak corresponds to direct reduction of bulk CuO crystallites to CuO because the reduction of bulk CuO is generally observed at ca. 520 K. In case of mixed ceria-zirconia solid solutions (e.g., 0.2CeZr, 0.5CeZr, and 0.8CeZr in this work), this peak is splitted into two peaks towards low temperatures (denoted as T_{r1} and T_{r2} for low- and high-temperature peaks). From literature [22–25], the peaks observed at T_{r1} and T_{r2} are ascribed to the reduction of highly dispersed CuO species strongly interacting with the support and the reduction of segregated CuO crystalline particles, respectively. The shift to low temperatures and the difference between T_{r1} and T_{r2} becomes larger as the *x* value increases from 0.2 to 0.8. This indicates that CuO particles supported on 0.8CeZr are the smallest, which is in good agreement with XRD results of CuO/*x*CeZr samples.

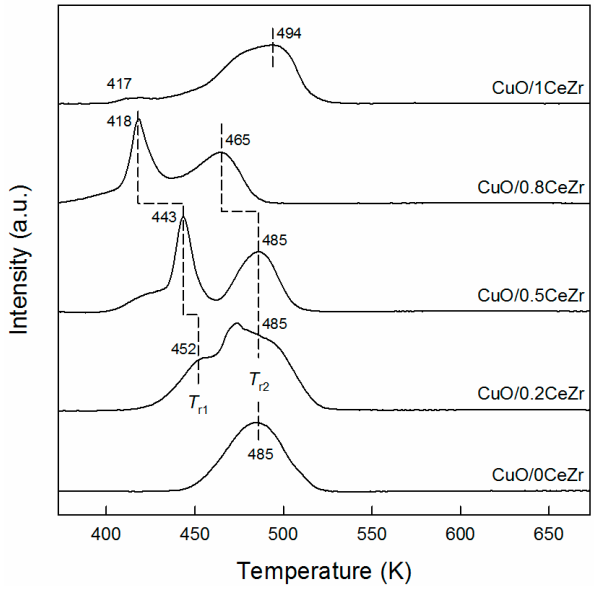

Figure 2. H_2 temperature-programmed reduction profiles of CuO/*x*CeZr samples.

Furthermore, N_2O-RFC experiment was conducted to evaluate a Cu dispersion (d_{Cu}), a specific Cu surface area (S_{Cu}), and a size of metallic Cu particles (D_{Cu}) for reduced Cu/*x*CeZr samples (Table 1). As the CeO_2 content increases the Cu dispersion increases from 2.5% for Cu/0CeZr to 11.9% for Cu/0.8CeZr and then dropped to 7.4% for Cu/1CeZr. The opposite trend is found for Cu particle size because smaller particles typically show higher fractions of exposed metal atoms at the surface.

Thus, the S_{Cu} value shows a volcano-type relationship against the Ce/(Ce + Zr) ratio with a maximum of 24.3 m^2 $g_{Cu}{}^{-1}$ for Cu/0.8CeZr. The Cu dispersion is closely associated with the extent of T_{r1} shift observed in H_2-TPR measurement; in other words, the sample with a higher Cu dispersion shows a lower T_{r1}. Particularly, the largest shift of T_{r1} is observed for CuO/0.8CeZr with the highest d_{Cu}. Therefore, the N_2O-RFC and H_2-TPR results suggest that the interaction of supported CuO and Cu species with ceria-zirconia surface is stronger for ceria-rich $Ce_xZr_{1-x}O_2$ supports. This is consistent with the report of Liu et al. for CuO/$Ce_xZr_{1-x}O_2$ catalysts in NO reduction that the ceria-rich phase cam interact more strongly with copper species than the zirconia-rich phase and thereby disperse metallic copper particles effectively [22].

Next, the densities of basic and acidic sites for reduced Cu/*x*CeZr samples on a per-gram-sample basis were measured by TPD experiments using CO_2 and NH_3 as a probe molecule, respectively. Figure 3a shows the desorption profiles of CO_2 detected using a TCD detector. All samples possess weak adsorption sites in 320–500 K associated with surface hydroxyl groups [26]. When a small amount of ZrO_2 is mixed with ceria, the amount of CO_2 desorbed above 450 K is enhanced, meaning a greater number of medium and strong CO_2 binding sites associated with M^{n+}–O^{2-} pairs and low coordination O^{2-} anions, respectively [27]. This also happens when a small amount of CeO_2 is mixed with zirconia. Thus, the relationship between the base site density (N_{CO2}) and the Ce/(Ce + Zr) ratio appears to be bimodal; the maximum N_{CO2} value is ca. 619.0 μmol g^{-1} for Cu/0.8CeZr and Cu/0.2CeZr (Table 1). On the other hand, the acid site density (N_{NH3}) of reduced Cu/*x*CeZr samples was measured using NH_3-TPD profiles shown in Figure 3b. When a small amount of CeO_2 is mixed with zirconia having Lewis acid sites generally, the total area for NH_3 desorption appears to be increased a little. The further addition of CeO_2 leads to a decrease in surface acidity. This is confirmed by the trend of N_{NH3} value against the Ce/(Ce + Zr) ratio with a maximum of 1183.2 μmol g^{-1} for Cu/0.2CeZr. (Table 1). However, it should be noted here that the N_{NH3} value measured in this work is a combination result of surface Cu species and *x*CeZr support, because acid sites can be generated by deposition of metallic Cu particles onto support materials [28,29]. For Pd/ceria-zirconia catalysts, surface acidity was reported to be associated primarily with zirconia and not with ceria and Pd particles [16].

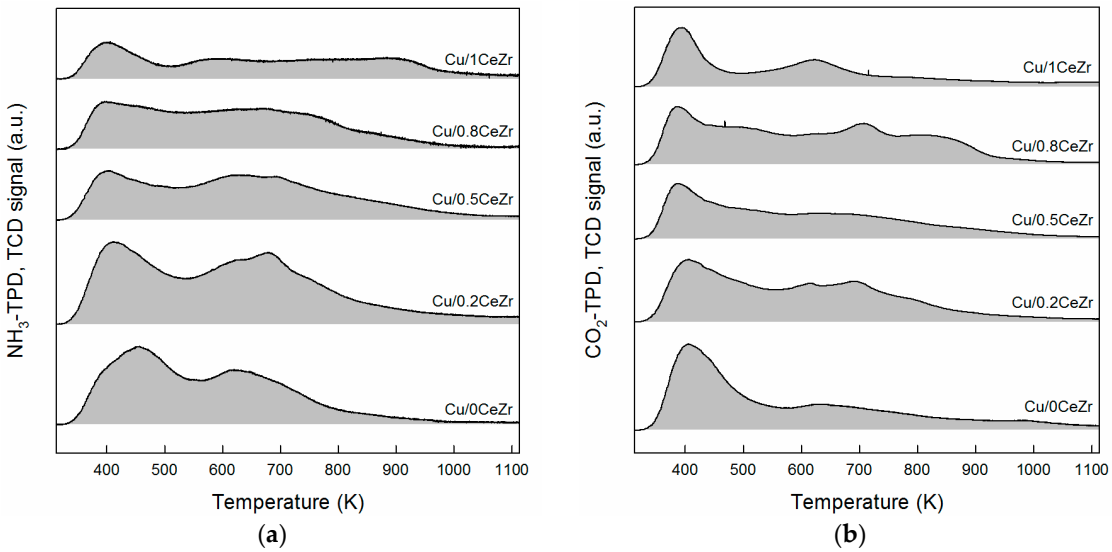

Figure 3. (**a**) NH_3 and (**b**) CO_2 temperature-programmed desorption profiles of Cu/*x*CeZr samples.

2.2. Catalytic Performance in the Cross-Aldol Condensation of Acetone and n-Butanol

The activity and selectivity results in the cross-aldol condensation of acetone and butanol over Cu/*x*CeZr catalysts with different *x* values are shown in Figure 4. The conversion of acetone, which is the limiting reactant in this work, is very similar as 38 ± 2.0% for Cu/1CeZr and Cu/0CeZr,

and it increases with the x value from 0.2 to 0.8. This means that an improved catalytic activity is obtained when more ceria is mixed with zirconia. Thus, the acetone conversion shows a volcano-type relationship against the Ce/(Ce + Zr) ratio with a maximum of 52.3% over Cu/0.8CeZr. Meanwhile, the major product in all catalytic runs is 2-heptanone produced by the cross-aldol condensation between acetone and *n*-butanol in an equimolar stoichiometry. Among the tested catalysts, Cu/0.8CeZr shows the lowest selectivity to 3-hepten-2-one (2.6%; the cross-aldol condensation product), the lowest selectivity to 2-heptanone (60.0%), and the highest selectivity to 6-undecanone (14.7%). Note here that 2-heptanone is the hydrogenation product of 3-hepten-2-one and it is alkylated to 6-undecanone once again by butyraldehyde formed by dehydrogenation of butanol. Therefore, it is understood that a high selectivity to 6-undecanone (C11) is due to enhanced catalytic performance in both the cross-aldol condensation and dehydrogenation/hydrogenation reactions. On the other hand, the production of butyl butyrate is observed over all tested catalysts, indicating that *n*-butanol reacts with butyric acid formed by disproportionation (Tishchenko) reaction of butyraldehyde due to the acidic/basic characters of support materials [30,31].

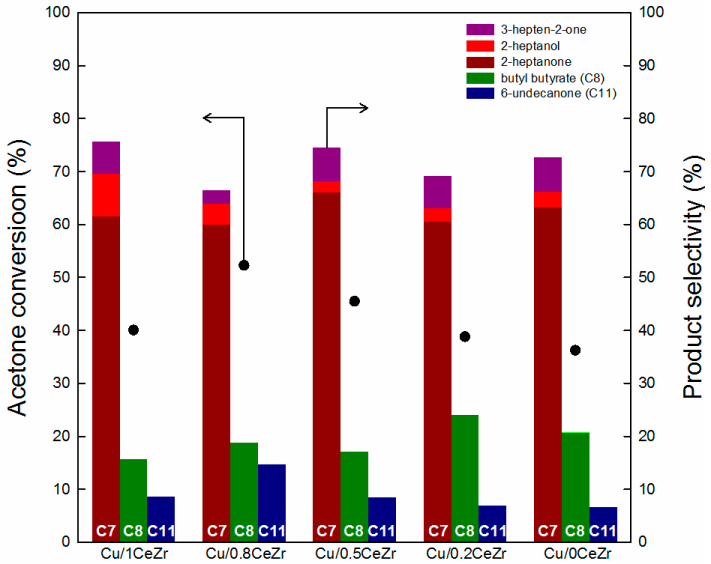

Figure 4. Acetone conversion and product selectivities of Cu/xCeZr catalysts. C7 includes 3-hepten-2-one, 2-heptanone, and 2-heptanol.

3. Discussion

3.1. Key Properties of Cu/xCeZr Catalysts in the Cross-Aldol Condensation of Acetone and n-Butanol

The activity and product selectivities are correlated with the specific Cu surface area (S_{Cu}) and acid/base site densities (N_{CO2} and N_{NH3}) of Cu/xCeZr catalysts. In Figure 5, the acetone conversion and the selectivity to major products, such as 2-heptanone, butyl butyrate and 6-undecanone, are plotted against the S_{Cu} value. The acetone conversion appears to be in a straight-line relationship with S_{Cu}. Since self-condensation products of acetone are rarely observed under the reaction condition employed in this work, acetone is consumed only by the cross-aldol condensation with butyraldehyde. This means that the conversion of acetone is efficient when more butyraldehyde (the dehydrogenation product of *n*-butanol) is produced. That is, the acetone conversion depends on available surface Cu atoms responsible for the dehydrogenation of *n*-butanol. Therefore, S_{Cu} is believed to be a principal contributor to the acetone conversion. This is supported by the fact that the other catalyst properties, i.e., the acid/base site densities, are not clearly related with the acetone conversion (Figure S1). For confirmation of the above discussion, basic MgO and acidic Al_2O_3 were used as a support material for Cu loading of 10 wt % same as Cu/xCeZr catalysts. The acetone conversion is 55.3% and 39.3% over Cu/MgO (S_{Cu} = 27.6 m^2 $g_{Cu}{}^{-1}$) and Cu/Al_2O_3 (S_{Cu} = 9.2 m^2 $g_{Cu}{}^{-1}$), respectively. As clearly

noticed in Figure 5a, the activity results of both catalysts against S_{Cu} are close to a fitted line, revealing again that S_{Cu} is the important catalyst property in determining the acetone conversion.

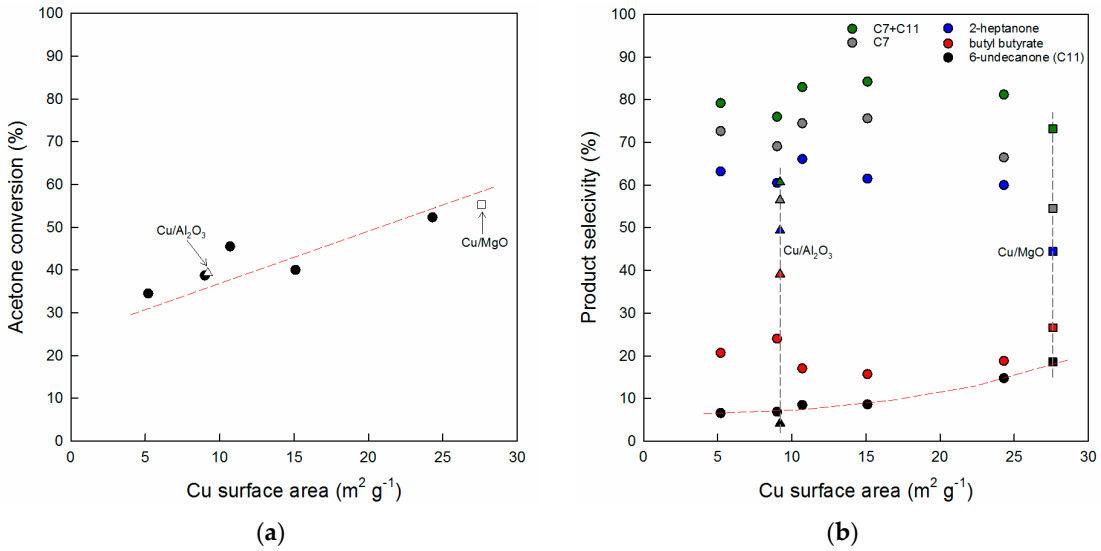

Figure 5. (**a**) Acetone conversion and (**b**) product selectivities plotted against the specific Cu surface area (S_{Cu}) of Cu/*x*CeZr (circles), Cu/MgO (squares), and Cu/Al_2O_3 (triangles) catalysts. C7 includes 3-hepten-2-one, 2-heptanone, and 2-heptanol.

On the other hand, the selectivity to 6-undecanone tends to increase with S_{Cu}, whereas the correlations between S_{Cu} and the selectivities to 2-heptanone and butyl butyrate are not good (Figure 5b). The former finding is consistent with the above explanation because the increased production of 6-undecanone from 2-heptanone is possible by a higher concentration of butyraldehyde achieved over more surface Cu atoms. This discussion is still appropriate even when the product selectivities over Cu/MgO and Cu/Al_2O_3 are considered together. However, since the latter observation is rather difficult to understand, a correlation work is further made between N_{NH3} and the product selectivities, as shown in Figure 6. The remarkable point to be addressed is that the selectivity to butyl butyrate increases with N_{NH3}. This means that its formation is dependent on acidic sites generally known to play a key role in the esterification reaction, which is supported by the high ester selectivity (39.1%) obtained over Cu/Al_2O_3 (N_{NH3} = 2053.9 μmol g^{-1}). Thus, the selectivity sum of mono-alkylation products (3-hepten-2-one, 2-heptanone, and 2-heptanol) and di-alkylation product (6-undecanone) decreases with increasing N_{NH3}.

However, we failed to find a good correlation between N_{CO2} and the selectivities to the major products (not shown for the sake of brevity), although aldol condensation reactions generally take place over basic sites. This may suggest that the production of cross-aldol condensation products is determined not only by basic sites but surface Cu atoms of supported Cu catalysts. Thus, the S_{Cu} value is multiplied by the N_{CO2} value for Cu/*x*CeZr catalysts, followed by normalization based on the value of Cu/MgO (N_{CO2} = 717.7 μmol g^{-1}) showing the highest calculation result. When the yields of cross-aldol condensation products are plotted against the normalized value (N_{dual}) in the range from 0 to 1, relatively good correlations are obtained, as presented in Figure 7. As the N_{dual} value increases, the total yield of C7 and C11 increases along with the C7 yield, indicating that the increased formation of cross-aldol condensation products is achieved possibly by a combination of Cu sites and basic sites. Although the similar increasing trend is observed for 2-heptanone, the other C7 products such as 3-hepten-2-one and 2-heptanol show different changes as a function of N_{dual} (Figure 7b). This is obviously due to more available surface Cu atoms for the hydrogenation reaction. In the case of 6-undecanone (di-alkylation product), a correlation is estimated to be linear with R^2 = 0.9661,

indicating that the yield of this product is a good measure in evaluating the dual catalytic performance in the cross-aldol condensation of acetone and *n*-butanol.

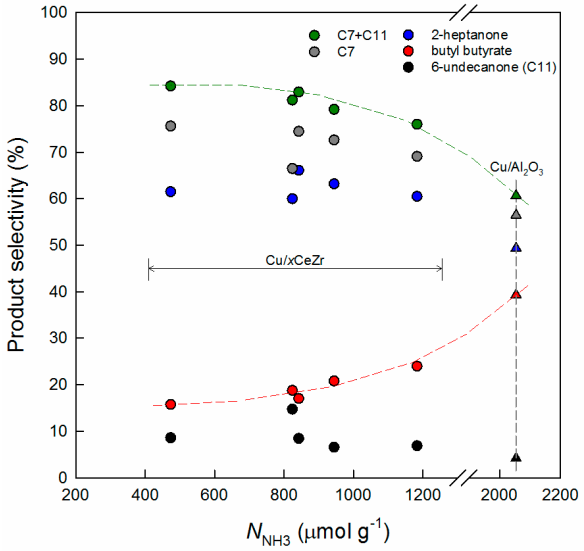

Figure 6. Product selectivities plotted against the acid site density (N_{NH3}) of Cu/*x*CeZr (circles) and Cu/Al_2O_3 (triangles) catalysts. C7 includes 3-hepten-2-one, 2-heptanone, and 2-heptanol.

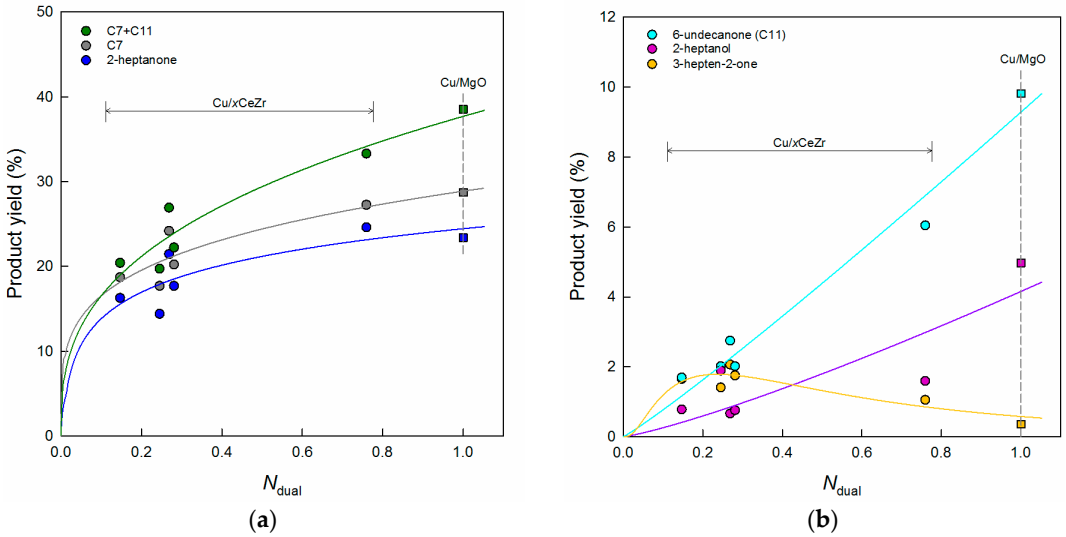

Figure 7. (**a**) Acetone conversion and (**b**) product selectivities plotted against the normalized value (N_{dual}) of Cu/*x*CeZr (circles) and Cu/MgO (squares) catalysts. C7 includes 3-hepten-2-one, 2-heptanone, and 2-heptanol.

3.2. Reaction Pathway in the Cross-Aldol Condensation of Acetone and n-Butanol over Cu/xCeZr

The above analysis suggests that surface Cu sites and acid/base sites should be well balanced for the selective production of cross-aldol condensation products, which is consistent with a recent report by Toste et al. [8]. First, surface Cu sites is inevitably necessary for the dehydrogenation of *n*-butanol into butyraldehyde. The next is the cross-aldol condensation over basic sites through enolate formation from acetone and subsequent attack of the electron-rich enolate to the electrophilic carbonyl carbon of butyraldehyde. The resulting ketol is transformed to 3-hepten-2-one by the dehydration reaction over acidic sites and further to 2-heptanone by the hydrogenation reaction over Cu sites. Furthermore, 2-heptanone is hydrogenated to 2-heptanol or it is alkylated once again into 6-undecanone via the above condensation.

The above-mentioned reaction pathway, reflected in Scheme 1, has been well documented for Cu/hydrotalcite catalysts [6–8]. Since the significant difference between hydrotalcite and ceria-zirconia is presumed to be a basic character, we conducted the condensation reaction of acetone and butyraldehyde over *x*CeZr without Cu. Interestingly, the acetone conversion is measured to be 4–6% for all support materials, including MgO and Al_2O_3. The similar conversion values (4–7%) are obtained in the acetone-butyraldehyde condensation reaction over Cu/*x*CeZr, Cu/MgO, and Cu/Al_2O_3. The low acetone conversion values in these experiments suggest that the adsorbed acyl species is formed from *n*-butanol by surface Cu particle and it, but not free aldehyde, then reacts with an acetone enolate supplied by acetone deprotonation over basic sites, yielding the cross-aldol condensation products. In this regard, the product distribution needs to be investigated because it depends on acidic/basic and metallic character of catalysts. Figure 8 shows the product selectivities obtained by the acetone-butyraldehyde condensation reaction over supported Cu catalysts. Unlike the condensation reaction between acetone and *n*-butanol, the detected products are 2-ethyl-2-hexenal (aldol condensation product of butyraldehyde), butyl butyrate (dehydrogenation product of hemiacetal formed by the reaction between *n*-butanol and butyraldehyde [8]), 3-hepten-2-one, and 2-heptanone, while there is no products by condensation of acetone. The former two products are formed by the condensation of butanol itself, while the others are the cross-aldol condensation products (denoted as C7 in Figure 8). All catalysts exhibit the selectivity to 2-ethyl-2-hexenal in the range from 50% to 77%, except Cu/MgO in which C7 is the majority. Among Cu/*x*CeZr catalysts, Cu/0.8CeZr shows the highest C7 selectivity of 40%. The common features in Cu/MgO and Cu/0.8CeZr are both high S_{Cu} and N_{CO2} values. This possibly explains that some of butyraldehyde (a strong electrophile) is adsorbed onto Cu surface, followed by the aldol condensation reaction with an acetone enolate over basic sites. This explanation is consistent to the catalytic performance discussed by the results in Figure 7.

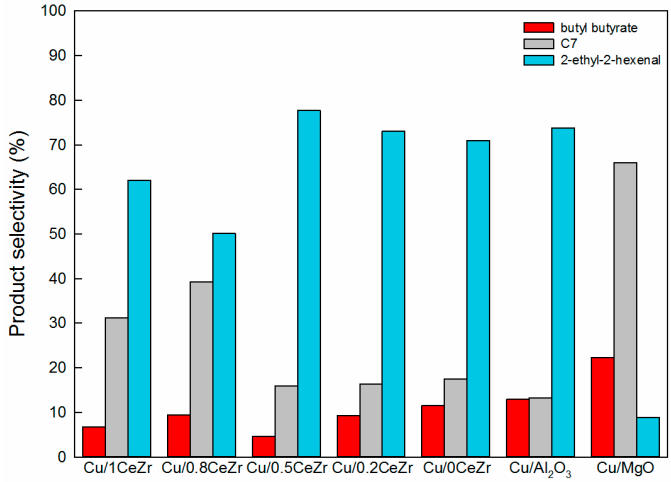

Figure 8. Product selectivities obtained in the reaction of acetone with butyraldehyde over Cu/*x*CeZr, Cu/Al_2O_3, and Cu/MgO catalysts.

3.3. Comparison of Cu/0.8CeZr and Cu/MgO Catalysts

From the activity results, Cu/MgO appears to be a better catalyst than Cu/0.8CeZr, the most active among the prepared Cu/*x*CeZr catalysts. Thus, the experiments as a function of reaction time were conducted for the two catalysts, as shown in Figure 9. For Cu/MgO the acetone conversion increases to 60% at about 2 h and further increase is not observed for a prolonged time. The similar time-dependent variation is obtained on the selectivities to butyl butyrate and 2-heptanol being stable at 26% and 10%, respectively. However, the selectivity to 2-heptanone decreases to 30% at 24 h and the selectivity to 6-undecanone increases to 32%, which is understood because the former product is consumed for the formation of di-alkylation product. On the other hand, Cu/0.8CeZr shows the

gradual increase in the acetone conversion to 63% at 24 h. Although the change in product selectivities is similar to that of Cu/MgO, the selectivities to 2-heptanone and 6-undecanone are measured to be both 39% at 24 h over Cu/0.8CeZr. Particularly, the selectivity to 6-undecanone increases linearly with time, which explains its improved formation at a longer reaction time than Cu/MgO. Since a higher selectivity to 2-heptanone and 6-undecanone is preferred in the cross-aldol condensation of acetone and *n*-butanol, Cu/0.8CeZr is believed to be more active than Cu/MgO.

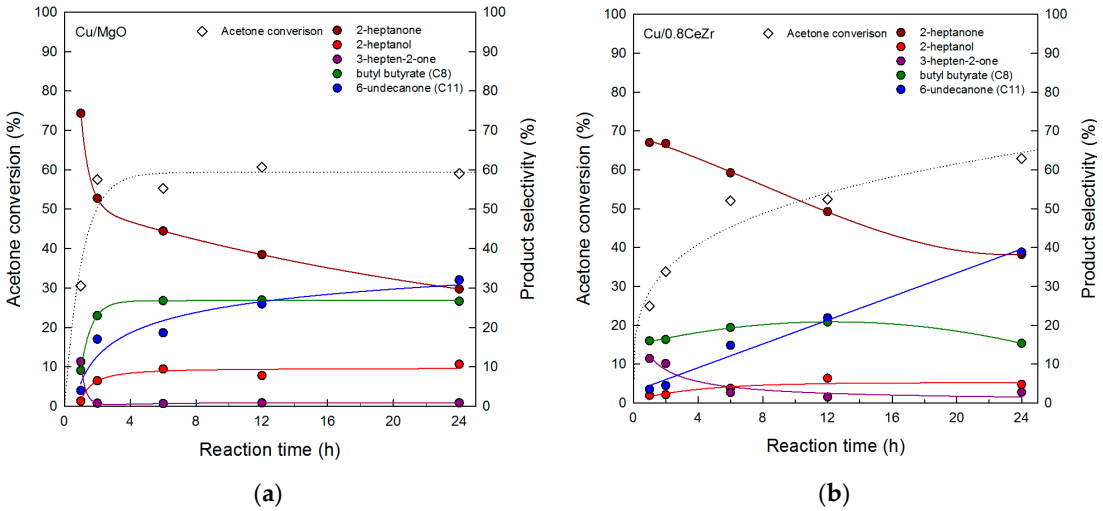

Figure 9. Acetone conversion and product selectivities plotted against the reaction time over (**a**) Cu/MgO and (**b**) Cu/0.8CeZr catalysts.

Additionally, we examined the catalyst stability by comparing XRD patterns of fresh (i.e., reduced) and spent Cu/MgO and Cu/0.8CeZr catalysts. As shown in Figure 10, the spent Cu/0.8CeZr displays very identical reflections to the fresh one, indicating that it is stable in the reaction. When Cu/0.8CeZr is repeatedly used for the 6-h reaction, the acetone conversion and product distribution are lower by 10% than the first-run result (not shown for brevity) but they are rather maintained in further repeated runs. However, the reflections of spent Cu/MgO are very different from those of the fresh one. The remarkable change from MgO to $Mg(OH)_2$ is due to water molecules formed by the aldol condensation reaction, which means that Cu/MgO is structurally unstable in the reaction.

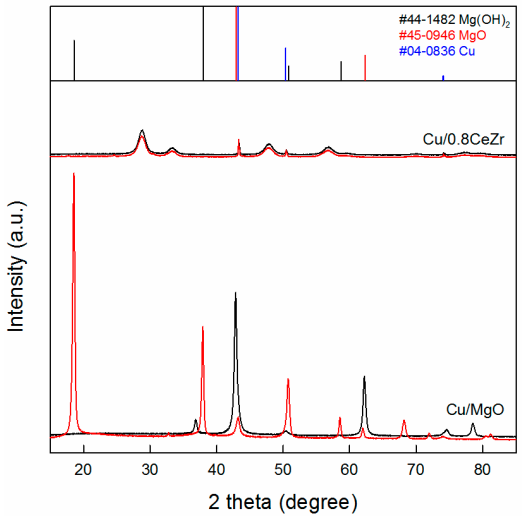

Figure 10. Powder X-ray diffraction patterns of fresh (black) and spent (red) Cu/0.8CeZr and Cu/MgO catalysts. The reflections of $Mg(OH)_2$ (black bars), MgO (red bars), and Cu metal (blue bars) are included for peak identification.

4. Experimental

4.1. Catalyst Preparation

$Ce_xZr_{1-x}O_2$ supports, denoted as *x*CeZr, were prepared via coprecipitation, where the *x* value is 1, 0.8, 0.5, 0.2, and 0. For the preparation of 0.5CeZr support, an aqueous solution (1.2 M of 50 mL) containing 13.29 g $Ce(NO_3)_2{\cdot}6H_2O$ (98%, Yakuri Pure Chemicals, Kyoto, Japan) and 7.08 g $ZrO(NO_3)_2{\cdot}nH_2O$ (Strem Chemicals, Newburyport, MA, USA) was added dropwise (15 mL min^{-1}) into NaOH solution (0.3 M, 600 mL) at 343 K under vigorous stirring. After complete addition, the resulting suspension was aged at 343 K for 24 h, filtered and washed repeatedly with deionized water. The so-obtained white cake was dried at 378 K overnight, followed by crushing and sieving to less than 200 μm. Finally, the calcination was carried out at 873 K (ramping rate 5 K min^{-1}) for 3 h in air. The other *x*CeZr samples were prepared in the same manner except the weights of $Ce(NO_3)_2{\cdot}6H_2O$ and $ZrO(NO_3)_2{\cdot}nH_2O$ added. MgO was also prepared via precipitation of $Mg(NO_3)_2{\cdot}6H_2O$ (2.4 M, 175 mL) with NaOH solution (0.24 M, 4200 mL), followed by calcination at 773 K (ramping rate 5 K min^{-1}) for 3 h in air. Al_2O_3 (BET surface area = 180 m^2 g^{-1}) was purchased from Strem Chemicals (Newburyport, MA, USA) and used without pretreatment.

Supported Cu catalysts of 10 wt % Cu loading were prepared by addition of aqueous Cu^{2+} solution (ca. 2 mL) containing 0.85 g $Cu(NO_3)_2{\cdot}3H_2O$ (99%, Daejung Chemicals & Metals, Siheung, Korea) into the support material (2 g) until the solid surface was pretty wet. The impregnated sample was dried at 378 K overnight and calcined at 673 K (ramping rate 5 K min^{-1}) for 3 h in air, resulting in CuO-loaded samples denoted as CuO/*x*CeZr, CuO/MgO, and CuO/Al_2O_3. The final catalysts, such as Cu/*x*CeZr, Cu/MgO, and Cu/Al_2O_3, were obtained by reduction of the calcined samples at 523 K for 3 h in a H_2 flow (100 cm^3 min^{-1}).

4.2. Catalyst Characterization

Powder XRD analysis was performed with a Rigaku MINIFlex 600 (Rigaku Corp., Spring, TX, USA) using a Cu Kα radiation source at 40 kV and 15 mA. The specific BET surface area of the sample (ca. 0.2 g) was measured at 77 K using a Micromeritics 3Flex (Micromeritics Instrument Corp., Norcross, GA, USA) after pretreatment at 373 K for 1 h under vacuum.

Experiments for temperature-programmed desorption of CO_2 and NH_3 were performed using a BELCAT-B (BEL Japan, Inc., Toyonaka, Japan) coupled with a BEL-Mass detector (BEL Japan, Inc., Toyonaka, Japan). Prior to CO_2 adsorption, CuO-loaded sample (50 mg) was reduced at 523 K for 3 h with 10% H_2/Ar (50 cm^3 min^{-1}) and cooled to 308 K under He. After 5% CO_2 in He was fed at 308 K for 30 min and purged with He for 2 h, CO_2-TPD experiment was started by heating to 1123 K at a rate of 10 K min^{-1} in a flow of He (30 cm^3 min^{-1}). For NH_3-TPD experiment, CuO-loaded sample (50 mg) was reduced in the same manner as for CO_2-TPD and then exposed to 5% NH_3/He at 308 K for 30 min. After purge with He for 2 h, NH_3-TPD experiment was started by heating to 1123 K at a rate of 10 K min^{-1} in a He flow (50 cm^3 min^{-1}). For H_2-TPR measurement conducted in a Micromeritics AutoChem 2910 (Micromeritics Instrument Corp., Norcross, GA, USA), the calcined sample (50 mg) was pretreated at 363 K in He and heated to 673 K at a rate of 5 K min^{-1} using 10% H_2 in Ar (50 sccm).

For measuring a specific Cu surface area, N_2O-RFC experiment was conducted in a BELCAT-B (BEL Japan, Inc., Toyonaka, Japan). After reducing a sample CuO/*x*CeZr (ca. 50 mg) at 523 K for 3 h with 10% H_2/Ar (30 cm^3 min^{-1}) and cooling to 313 K under He, 1% N_2O/He (5 cm^3 min^{-1}) was introduced and the released nitrogen (m/z = 28) was measured by a MS detector. The calculation was based on the reaction stoichiometry between copper and oxygen (Cu/O = 2) and the copper surface density of 1.46×10^{19} Cu atom m^{-2}.

4.3. Activity Test

Catalytic experiments for the cross-aldol condensation of acetone and *n*-butanol were conducted in a stainless-steel batch reactor (total volume 150 cm^3: Hanwoul Engineering, Gunpo, Korea) into

which the reduced Cu catalyst (0.5 g), acetone (194 mmol), and *n*-butanol or butyraldehyde (388 mmol) were charged. After N_2 purge to remove oxygen and moisture inside, the reaction mixture was heated to 513 K at a rate of 10 K min^{-1}. The reaction was conducted at 513 K for 6 h under N_2 where the reactor pressure was nearly constant at 25 bar. Note that the reaction condition is very similar to that in the report of Toste et al. [5]. The product sample was taken out, filtered through a ADVANTEC® syringe filter (0.45 μm diameter; Toyo Roshi Kaisha, Ltd., Tokyo, Japan) and mixed with an internal standard cyclohexane. This mixture was analyzed with a Younglin YL6100 gas chromatograph (Younglin Instrument, Anyang, Korea) equipped with a FID detector (Younglin Instrument, Anyang, Korea) and an HP-INNOWAX column (50 m, 0.2 mm, 0.4 μm; Agilent Technologies, Santa Clara, CA, USA). The acetone conversion was calculated by the molar difference between the initial charge and the remaining acetone. The quantitative selectivities to products such as 3-hepten-2-one, 2-heptanone, 2-heptanol, butyl butyrate, and 6-undecanone were calculated on the basis of the following equation: selectivity to product *i* [mol%] = (mole of product *i*)/(mole of all products in the reaction mixture) × 100%.

5. Conclusions

Among Cu/*x*CeZr catalysts, Cu/0.8CeZr produces the cross-aldol condensation products (all C7 plus C11) in the largest amount. The enhanced catalytic performance in the reaction of acetone and *n*-butanol is a combination result of more surface Cu atoms and more base sites responsible for the alcohol dehydrogenation and aldol condensation reactions, respectively. This is confirmed by the results obtained in the condensation of acetone and butyraldehyde over Cu/0.8CeZr and Cu/MgO. Since the conversion of acetone is less efficient in the reaction with butyraldehyde, it is suggested that the dehydrogenation product of *n*-butanol exist in a form of acyl species adsorbed onto Cu surface, not free aldehyde, followed by undergoing the condensation reaction with an acetone enolate formed by acetone deprotonation over basic sites. Although Cu/MgO shows the comparable cross-aldol condensation activity to Cu/0.8CeZr, MgO is transformed into $Mg(OH)_2$ by water formed by the condensation reaction. Consequently, Cu supported on ceria-zirconia of ceria rich is catalytically active and stable in the cross-aldol condensation of acetone and *n*-butanol.

Supplementary Materials: The following are available online at www.mdpi.com/2073-4344/7/9/249/s1, Figure S1: Correlation of acetone conversion with (a) N_{NH3} and (b) N_{CO2} of Cu/*x*CeZr (circles), Cu/MgO (square), and Cu/Al_2O_3 (triangle) catalysts.

Acknowledgments: The authors acknowledge the financial support from the New & Renewable Energy Core Technology Program through the Korea Institute of Energy Technology Evaluation and Planning under the Ministry of Trade, Industry & Energy, Republic of Korea (KETEP-20143030091040), and from the Basic Science Research Program through the National Research Foundation of Korea under the Ministry of Education (NRF-2016R1A6A1A03013422). The former funding source covers the cost to publish in open access.

Author Contributions: Y.-W.S. conceived and designed the experiments; M.K. and J.P. performed the experiments; M.K. and H.P.R.K. analyzed the data; M.K. and J.P. contributed reagents/materials/analysis tools; M.K., H.P.R.K. and Y.-W.S. wrote the paper.

Conflicts of Interest: The authors declare no conflict of interest.

References

1. McKendry, P. Energy production from biomass (part 2): Conversion technologies. *Bioresour. Technol.* **2002**, *83*, 47–54. [CrossRef]
2. Eggeman, T.; Verser, D. The importance of utility systems in today's biorefineries and a vision for tomorrow. *Appl. Biochem. Biotechnol.* **2006**, *129–132*, 361–381. [CrossRef]
3. Granda, C.B.; Zhu, L.; Holtzapple, M.T. Sustainable liquid biofuels and their environmental impact. *Environ. Prog.* **2007**, *26*, 233–250. [CrossRef]
4. Breitkreuz, K.; Menne, A.; Kraft, A. New process for sustainable fuels and chemicals from bio-based alcohols and acetone. *Biofuels Bioprod. Biorefin.* **2014**, *8*, 504–515. [CrossRef]

5. Anbarasan, P.; Baer, Z.C.; Sreekumar, S.; Gross, E.; Binder, J.B.; Blanch, H.W.; Clark, D.S.; Toste, F.D. Integration of chemical catalysis with extractive fermentation to produce fuels. *Nature* **2012**, *491*, 235–239. [CrossRef] [PubMed]
6. Sreekumar, S.; Baer, Z.C.; Gross, E.; Padmanaban, S.; Goulas, K.; Gunbas, G.; Alayoglu, S.; Blanch, H.W.; Clark, D.S.; Toste, F.D. Chemocatalytic upgrading of tailored fermentation products toward biodiesel. *ChemSusChem* **2014**, *7*, 2445–2448. [CrossRef] [PubMed]
7. Goulas, K.A.; Sreekumar, S.; Song, Y.; Kharidehal, P.; Gunbas, G.; Dietrich, P.J.; Johnson, G.R.; Wang, Y.C.; Grippo, A.M.; Grabow, L.C.; et al. Synergistic effects in bimetallic palladium-copper catalysts improve selectivity in oxygenate coupling reactions. *J. Am. Chem. Soc.* **2016**, *138*, 6805–6812. [CrossRef] [PubMed]
8. Goulas, K.A.; Gunbas, G.; Dietrich, P.J.; Sreekumar, S.; Grippo, A.; Chen, J.P.; Gokhale, A.A.; Toste, F.D. ABE condensation over monometallic catalysts: Catalyst characterization and kinetics. *ChemCatChem* **2017**, *9*, 677–684. [CrossRef]
9. Gangadharan, A.; Shen, M.; Sooknoi, T.; Resasco, D.E.; Mallinson, R.G. Condensation reactions of propanal over $Ce_xZr_{1-x}O_2$ mixed oxide catalysts. *Appl. Catal. A* **2010**, *385*, 80–91. [CrossRef]
10. Di Cosimo, J.I.; Torres, G.; Apesteguia, C.R. One-step MIBK synthesis: A new process from 2-propanol. *J. Catal.* **2002**, *208*, 114–123. [CrossRef]
11. Hakim, S.H.; Shanks, B.H.; Dumesic, J.A. Catalytic upgrading of the light fraction of a simulated bio-oil over $CeZrO_x$ catalyst. *Appl. Catal. B* **2013**, *142–143*, 368–376. [CrossRef]
12. Postole, G.; Chowdhury, B.; Kramakar, B.; Pinki, K.; Banerji, J.; Auroux, A. Knoevenagel condensation reaction over acid—Base bifunctional nanocrystalline $Ce_xZr_{1-x}O_2$ solid solutions. *J. Catal.* **2010**, *269*, 110–121. [CrossRef]
13. Gaertner, C.A.; Serrano-Ruiz, J.C.; Braden, D.J.; Dumesic, J.A. Catalytic coupling of carboxylic acids by ketonization as a processing step in biomass conversion. *J. Catal.* **2009**, *266*, 71–78. [CrossRef]
14. Gaertner, C.A.; Serrano-Ruiz, J.C.; Braden, D.J.; Dumesic, J.A. Ketonization reactions of carboxylic acids and esters over ceria-zirconia as biomass-upgrading processes. *Ind. Eng. Chem. Res.* **2010**, *49*, 6027–6033. [CrossRef]
15. Kunkes, E.L.; Gürbüz, E.I.; Dumesic, J.A. Vapour-phase C–C coupling reactions of biomass-derived oxygenates over $Pd/CeZrO_x$ catalysts. *J. Catal.* **2009**, *266*, 236–249. [CrossRef]
16. Gürbüz, E.I.; Kunkes, E.L.; Dumesic, J.A. Integration of C–C coupling reactions of biomass-derived oxygenates to fuel-grade compounds. *Appl. Catal. B* **2010**, *94*, 134–141. [CrossRef]
17. Kunkes, E.L.; Simonetti, D.A.; West, R.M.; Serrano-Ruiz, J.C.; Gärtner, C.A.; Dumesic, J.A. Catalytic conversion of biomass to monofunctional hydrocarbons and targeted liquid-fuel classes. *Science* **2008**, *322*, 417–421. [CrossRef] [PubMed]
18. Faba, L.; Díaz, E.; Ordóñez, S. One-pot aldol condensation and hydrodeoxygenation of biomass-derived carbonyl compounds for biodiesel synthesis. *ChemSusChem* **2014**, *7*, 2816–2820. [CrossRef] [PubMed]
19. Requies, J.; Güemez, M.B.; Maireles, P.; Iriondo, A.; Barrio, V.L.; Cambra, J.F.; Arias, P.L. Zirconia supported Cu systems as catalysts for *n*-butanol conversion to butyraldehyde. *Appl. Catal. A* **2012**, *423–424*, 185–191. [CrossRef]
20. Zhang, F.; Chen, C.H.; Hanson, J.C.; Robinson, R.D.; Herman, I.P.; Chan, S.-W. Phases in ceria-zirconia binary oxide $(1-x)CeO_2-xZrO_2$ nanoparticles: The effect of particle size. *J. Am. Ceram. Soc.* **2006**, *89*, 1028–1036. [CrossRef]
21. Reddy, B.M.; Bharail, P.; Saikia, P.; Park, S.-E.; van den Berg, M.W.E.; Muhler, M.; Grünert, W. Structural characterization and catalytic activity of nanosized $Ce_xM_{1-x}O_2$ (M = Zr and Hf) mixed oxides. *J. Phys. Chem. C* **2008**, *112*, 11729–11737. [CrossRef]
22. Liu, L.; Yao, Z.; Liu, B.; Dong, L. Correlation of structural characteristics with catalytic performance of $CuO/Ce_xZr_{1-x}O_2$ catalysts for NO reduction by CO. *J. Catal.* **2010**, *275*, 45–60. [CrossRef]
23. Zou, Z.-Q.; Meng, M.; Guo, L.-H.; Zha, Y.-Q. Synthesis and characterization of $CuO/Ce_{1-x}Ti_xO_2$ catalysts used for low-temperature CO oxidation. *J. Hazard. Mater.* **2009**, *163*, 835–842. [CrossRef] [PubMed]
24. Moretti, E.; Lenarda, M.; Riello, P.; Storaro, L.; Talon, A.; Frattini, R.; Reyes-Carmona, A.; Jiménez-López, A.; Rodríguez-Castellón, E. Influence of synthesis parameters on the performance of CeO_2-CuO and CeO_2-ZrO_2-CuO systems in the catalytic oxidation of CO in excess of hydrogen. *Appl. Catal. B* **2013**, *129*, 556–565. [CrossRef]

25. Das, D.; Llorca, J.; Dominguez, M.; Colussi, S.; Trovarelli, A.; Gayen, A. Methanol steam reforming behavior of copper impregnated over CeO_2-ZrO_2 derived from a surfactant assisted coprecipitation route. *Int. J. Hydrog. Energy* **2015**, *40*, 10463–10479. [CrossRef]
26. Di Cosimo, J.I.; Apesteguía, C.R.; Ginés, M.J.L.; Iglesia, E. Structural requirements and reaction pathways in condensation reactions of alcohols on Mg_yAlO_x catalysts. *J. Catal.* **2000**, *190*, 261–275. [CrossRef]
27. Díez, V.K.; Di Cosimo, J.I.; Apesteguía, C.R. Study of the citral/acetone reaction on Mg_yAlO_x oxides: Effect of the chemical composition on catalyst activity, selectivity and stability. *Appl. Catal. A* **2008**, *345*, 143–151. [CrossRef]
28. Subbaramaiah, V.; Srivastava, V.C.; Mall, I.D. Optimization of reaction parameters and kinetic modeling of catalytic wet peroxidation of picoline by Cu/SBA-15. *Ind. Eng. Chem. Res.* **2013**, *52*, 9021–9029. [CrossRef]
29. Sagar, G.V.; Rao, P.V.R.; Srikanth, C.S.; Chary, K.V.R. Dispersion and reactivity of copper catalysts supported on Al_2O_3-ZrO_2. *J. Phys. Chem. B* **2006**, *110*, 13881–13888. [CrossRef] [PubMed]
30. Wang, X.; Saleh, R.Y.; Ozkan, U.S. Reaction network of aldehyde hydrogenation over sulfided Ni–Mo/Al_2O_3 catalysts. *J. Catal.* **2005**, *231*, 20–32. [CrossRef]
31. Wawrzetz, A.; Peng, B.; Hrabar, A.; Jentys, A.; Lemonidou, A.A.; Lercher, J.A. Towards understanding the bifunctional hydrodeoxygenation and aqueous phase reforming of glycerol. *J. Catal.* **2010**, *269*, 411–420. [CrossRef]